JOURNAL OF SOLID STATE CHEMISTRY 75, 30–40 (1988)

Trilithium Tetradecaboride Li_3B_{14}: Synthesis, Structure, and Properties*

G. MAIR, R. NESPER, AND H. G. VON SCHNERING

Max–Planck–Institut für Festkörperforschung, D-7000 Stuttgart 80, Heisenbergstrasse 1, West Germany

Received July 31, 1987

1. Introduction

Lithium boron compounds are of some interest, e.g., with respect to general structural relations to the Zintl polyanionic phases, as well as to the boranes, with respect to the physical and chemical properties affected by the high mobility of lithium (ionic conductivity, topochemical reactions), and with respect to the technical applications (battery technology, neutron scattering techniques).

On the right of the Zintl border, the elements form numerous binary compounds with the alkali metals (*1–4*), and their structures are well understood by the simple valence rules developed by Zintl (*5*), Klemm (*6*), and Mooser and Pearson (*7*). The lithium-rich phases exhibit some problems and it was indicated that the above cited rules may not be valid with lithium (*2, 3*). We have recently shown how a consistent valence description can be formulated even for lithium phases (*8–12*).

On the left of the Zintl border, the 3B elements especially form the classical Zintl phase, e.g., NaTl; but, on the other hand, they show typical characteristics of intermetallic phases. Important work was done in this field by Thümmel and Klemm (*13*), by Stöhr and Schäfer (*14*), and by Belin and Ling (*15*). In this connection, the lack of information about alkali metal borides is conspicuous. This obviously results from the considerable experimental difficulties: (i) the extreme differences of the melting points of the components; (ii) the high reactivity of both components with tube materials, especially at higher temperatures. Binary lithium borides have been investigated by several authors, but none of these phases is well characterized: $LiB_{10.85}$ (*16*), LiB_3 (*17*), LiB (*18*), $Li_{\sim 1}B$ (*19*), Li_7B_6 (*17*), Li_5B_4 (*20*), and Li_2B (*19*). Not even one single-crystal structure investigation is available and the only reasonable structural model is that of Li_5B_4 which was proposed from X-ray powder data. A recent review is given in (*21*). These unreliable results and the questionable characterization of the lithium borides stimulated our reinvestigation of the binary Li–B system (*22*). We have identified three new phases on the boron-rich side, but could not confirm any of the older results (*22*). A careful comparison

* Dedicated to Professor A. Rabenau on the occasion of his 65th birthday.

0022-4596/88 $3.00

of all experimental data reported earlier with our results show that some so-called compounds are obviously phase mixtures. We report here the boron richest compound $Li_3B_{14} = LiB_{4.67}$.

2. Experimental Problems

Lithium starts to react with boron at 650 K, yielding powder samples of poor quality. X-ray powder patterns show only a few weak reflections; the samples look dull and are mostly heterogeneous. Results from our experiments show that equilibrium conditions and crystals of good quality are reached very slowly at $T < 1200$ K. This is in agreement with observations cited above (*16–20*). The synthesis of well-crystallized samples requires temperatures above 1200 K on a time scale of 1 day to 1 week. Under these conditions, the usual container materials (Fe, Nb, Ta, Mo, BN) are attacked by Li or B or both. Furthermore, the purity of commercially available boron is not very high due to its affinity to traces of C, H, N, O, Al, etc. The formation of pure phases and larger crystals may be affected by the formation of other phases with such impurities.

In a series of experiments we found that the main difficulties can only be overcome by a combination of container materials. The reactions are best performed in molybdenum crucibles sealed in niobium ampoules, which are kept under argon in an alumina tube. Under these conditions niobium is fairly stable against lithium and can easily be used for sealed ampoules, but it is attacked rapidly by boron at reaction temperature, yielding brittle surface layers (niobium borides). Therefore, a direct contact of Nb and B must be avoided. Under the same conditions, molybdenum reacts much slower with boron, but recrystallizes considerably, giving rise to cracks in the container wall and an evaporation of lithium and can thus only be used as crucible.

3. Synthesis of Li_3B_{14}

Commercial β-rhombohedral boron (99.4%, Ventron) and lithium (99.9%, Alpha Products) were purified before usage. Boron was heated to 1250 K (10^{-1} Pa) for 10 to 20 hr to separate volatile impurities. Lithium was distilled in a water-cooled steel apparatus (870 K, 10^{-4} Pa). Reactants and products were handled in a dry-box (Braun) under argon atmosphere. The molybdenum crucible was machined from a rod of about 6 mm radius and 70 mm length (1.5-mm wall) and cleaned mechanically in a sand beam.

Li_3B_{14} is prepared from a stoichiometric mixture of the elements. A slight excess of boron (~3%) is recommended to account for surface reactions of molybdenum with boron. The molybdenum crucible is loaded with 100 mg Li and 780 mg B and sealed into a niobium ampoule under 10^4 Pa argon by arc-welding (Nb tube of about 90–100 mm length; ϕ = 12 mm; 1-mm wall). The ampoule is heated inside an alumina tube (after evacuation filled by argon; 10^5 Pa) up to 1700 K with a rate of 400 K/hr, kept at this temperature for 12 hr, and cooled down for approximately 10 hr to room temperature. The reaction product is homogeneous and well crystallized.

Li_3B_{14} forms compact polyhedral crystals which are transparent red in transmission, but look black in reflecting light. The characteristic X-ray powder pattern is shown in Fig. 1. The chemical analysis was carried out by atomic emission spectroscopy (ICP, ARL) and gives a composition of $LiB_{4.8\pm0.2}$ (calcd $LiB_{4.67}$).

4. Physical Properties

The electrical conductivity of Li_3B_{14} was measured on a compressed powder sample. Three hundred milligrams were compacted in a stainless-steel press at 6×10^8 Pa to a pellet of 10 mm diameter. This is a rather

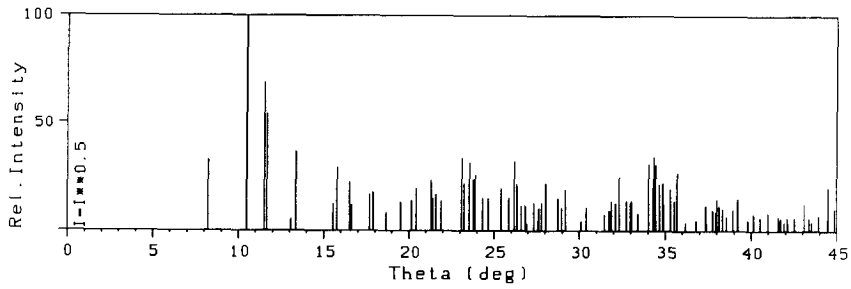

FIG. 1. Calculated X-ray powder pattern for Li_3B_{14} (Guinier geometry, $\lambda(CuK\alpha_1) = 154.056$ pm, $\theta_{max} = 45°$, (23)).

difficult procedure due to the brittleness of Li_3B_{14}. No binders or lubricants were added. The pellet was inserted between Mo inert electrodes and investigated from 298 to 900 K by a frequency dependent measurement of the direct current (DC) conductivity and the alternate current (AC) complex transmittance in the range 4 Hz to 150 kHz (*24, 25*). Li_3B_{14} shows a mixed ionic (Li^+) and electronic conductivity with $\sigma_{overall} = 4 \times 10^{-4}\ \Omega^{-1}\ cm^{-1}$ at 770 K and an activation energy of $E_A = 1.6$ eV for the range between 600 and 900 K (Fig. 2). In the lower temperature region from 290 to 600 K an extrinsic conductivity due to an impurity band with $E_A = 0.15$ eV and ρ_{ex} (400 K) $= 10^{-6}\ \Omega^{-1}\ cm^{-1}$ dominates. Very low conductivity ρ_{ex} with respect to $E_{A_{ex}}$ and the occurrence of much higher activation energy at higher temperatures gives rise to this interpretation. For the whole range of investigation, the electronic conductivity dominates over the ionic conductivity, e.g., no difference between AC and DC current occurs.

5. Chemical Properties; Topochemical Reactions

Li_3B_{14} reacts very slowly with H_2O, but more rapidly with strong acids under evolution of H_2. The morphology of single crystals is preserved and the reaction was shown to be strictly topotactical, leaving the boron framework of the structure unchanged. The transformed crystals have a Li/B ratio according to $Li_{3-x}B_{14}$ with $x \leq 1.7$. The limiting value of x has been proven by three independent reactions, namely (i) by the reaction with H_2O, (ii) by the coulometric titration, and (iii) by the thermal decomposition.

(*i*) *Reaction with H_2O and acids*

Li_3B_{14} reacts with protons according to

$$Li_3B_{14} + xH^+ = Li_{3-x}B_{14} + \frac{x}{2} H_2 + xLi^+.$$

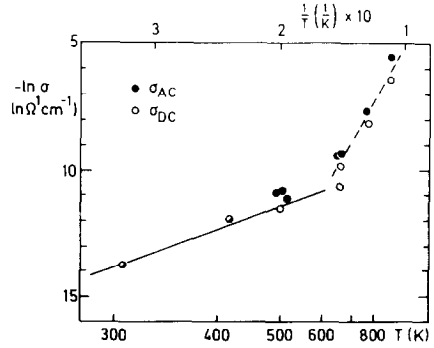

FIG. 2. Temperature dependence of the electrical conductivity of Li_3B_{14} (open circles, direct current; solid circles, alternating current). In the low-temperature region up to 450 K there is mainly electronic and in the higher region mixed electronic and ionic conductivity. The band gap in the lower region amounts to $E_g = 0.15$ eV and is probably due to impurities ρ_{el} (290 K) $= 9 \times 10^{-7}\ \Omega^{-1}\ cm^{-1}$. For the higher temperature range $E_g = 1.6$ eV for the mixed conductivity ($\rho_{tot} = 4 \times 10^{-4}\ \Omega^{-1}\ cm^{-1}$).

After a 1-hr reaction with half-concentrated sulfuric acid, the reaction product was analyzed chemically to be $Li_{1.3}H_{0.4}O_{0.6}B_{14}$. The crystallinity is preserved and a single-crystal study shows only one remarkable change in the boron cage distances as well as an increase in the disorder at the Li positions (cf. Sections 6 and 7).

(*ii*) *Coulometric Titration*

The coulometric titration of Li_3B_{14} was performed at 720 K with the electric cell Mo, Li_3B_{14}/LiCl, KCl/Li_xAl, Al, Mo (*22*). The ionic conductor is an eutectic melt of LiCl and KCl; the method has been described elsewhere (*26–29*). Thirty milligrams Li_3B_{14} were placed in a basket of Mo sheet (0.1 mm thickness) together with a Mo wire (0.2 mm diameter) to enhance the electric contact with powder sample and compressed with pliers. In the first step, the Li_xAl electrode was prepared by titration of lithium into an Al block of 0.5 g up to a composition of $Li_{0.4}Al$. This procedure allows a purification of the eutectic melt from minor impurities (oxygen, water, etc.).

The measurements were performed at 720 K in the voltage range 0–2.7 V vs lithium (limited by the decomposition of the eutectic melt). Figure 3 shows a typical experiment. The equilibrium potential of Li_3B_{14} vs lithium is about 800 mV. The compound is stable at 720 K against lithium which is deposited on the surface.

The reaction $Li_3B_{14} \xrightarrow{-Li} Li_{3-x}B_{14}$ is reversible and is accompanied by changes of the equilibrium potential. One-sixth of the Li content can be removed, preserving the boron framework of Li_3B_{14}. The equilibrium potential of $Li_{2.5\pm0.1}B_{14}$ vs lithium is about 1700 mV. It is very likely that this composition marks the complete depopulation of one Li site (Li2, compare Section 7). With decreasing Li concentration the potential increases continuously. At the limiting voltage of 2700 mV a composition of $Li_{1.3\pm0.3}B_{14}$ is reached. Further decrease of the ratio Li : B causes a breakdown of the crystalline state, which is accompanied by a step in the potential (Fig. 3). The latter product does not show any X-ray diffraction lines and is expected to be amorphous.

(*iii*) *Thermal Decomposition*

The thermal decomposition of Li_3B_{14} was studied on a thermobalance (Netzsch) coupled to a mass spectrometer (quadrupole technique, Balzers). The decomposition shows two steps at 1200 and 1450 K. The first corresponds to the formation of $Li_{\sim 2}B_{14}$ and the second to the formation of α-rhombohedral boron. The corresponding mass spectra show only lithium in the gaseous phase, but give no indication of particles containing boron.

X-ray powder pattern of the samples from reaction (i) = $Li_{1.3}H_{0.4}O_{0.6}B_{14}$, (ii) = $Li_{1.3}B_{14}$, and (iii) = $Li_{\sim 2}B_{14}$ are nearly identical resembling the Li_3B_{14} diagram (Fig. 1) very much. Going beyond the composition $Li_{1.3}B_{14}$ to lower lithium content gives rise to amorphous samples and/or β-rhombohedral boron. Obviously the B_{14}-frame is not stable under those conditions.

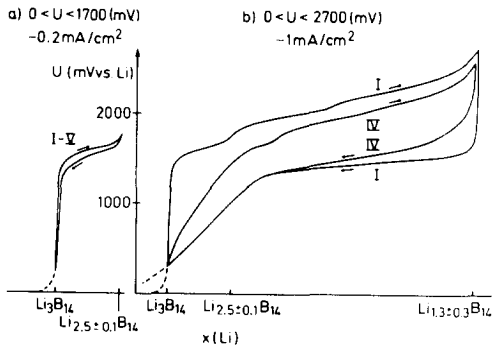

FIG. 3. Coulometric titration of Li_3B_{14} at 720 K. The roman numbers indicate the redox cycles of Li_3B_{14}–$Li_{1.3}B_{14}$. At the left side the redox titration Li_3B_{14}–$Li_{2.5}B_{14}$ is shown which exhibits a much smaller hysteresis than that of the large redox reaction.

TABLE I

CRYSTAL DATA, DATA COLLECTION, AND STRUCTURE DETERMINATION

Formula	Li_3B_{14}	$Li_{3-x}B_{14}$ ($x \approx 1.2$)
Mole weight (amu)	172.17	163.84
Temperature (K)	298	298
Space group (Nr.)	$I42d$-C_{2d}^{12}	(Nr. 122)
Lattice constants (pm)		
a	1076.4(53)	1071.4(51)
c	894.7(4)	892.6(4)
c/a	0.8312	0.8331
Volume (10^6 pm^3)	1036.6	1024.6
Mole volume (cm^3 mole^{-1})	129.58	128.08
Cell contents	8	8
Density (g cm^{-3})	2.206(3)	2.12
μ(Mo$K\alpha$) (cm^{-1})	0.6	0.6
Measurement	Four circle diffractometer (SYNTEX P$\bar{1}$); graphite monochromator; scintillation counter; λ(Mo$K\alpha$) = 71.069 (pm); $3.5° \leq 2\theta \leq 55.0°$; ω-scan; variable speed dependent on I; empirical absorption correction (ψ-scan, 10 reflections).	
Structure determination	Direct methods (SHELXTL (*31*)); full matrix least-squares procedure (SHELX76 (*31*)); weight: σ^{-2}	
$N(hkl)$	375	382
$N'(hkl)$	334 with $F_o > 3\sigma(F_o)$	335 with $F_o > 3\sigma(F_o)$
n (parameter)	93	84
R (aniso)	0.035	0.052
R_w (aniso)	0.033	0.050
R_w (aniso, $2\theta \geq 30°$)	0.029	

6. Crystal Structure Analysis

The crystal structures of Li_3B_{14} and of the reaction product $Li_{1.3}H_{0.4}O_{0.6}B_{14}$ were determined by single-crystal methods. The crystallographic data are listed in Table I. The lithium positions were found by subsequent Fourier and difference Fourier synthesis. None of these sites are fully occupied. The occupancy of three sites is 50% with good accuracy (Li1, Li3, Li4). This is a necessity because the corresponding distances do not allow for a full occupancy of all sites (compare Table IV). For the Li2 site only a population of about 40% seems to be most likely due to the X-ray data. The refinement of thermal parameters as well as of site occupation factors at the Li positions was carried out with the full data set. The refinement of the occupancies and anisotropic temperature factors yield slightly smaller values than $\frac{1}{2}$ for Li1, 2, 3, which are, however, in the range of the given standard deviations. Due to the relatively low electron density of the boron core, the positional boron parameters were redetermined only by the 270 reflections (Li_3B_{14}) with $2\theta > 30°$ to avoid bias of the core parameters by the valence electron distribution. Parameters and interatomic distances are listed in Tables II–IV.

TABLE II

ATOMIC POSITIONAL PARAMETERS, EQUIISOTROPIC (B1–B7, MARKED BY *), AND ISOTROPIC TEMPERATURE FACTORS (Li1–Li4) (PM^2) FOR Li_3B_{14} (FIRST ROW, CONVENTIONAL REFINEMENT; SECOND ROW, REFINEMENT FOR $2\theta \geq 30°$) AND FOR $Li_{3-x}B_{14}$ (THIRD ROW)

Atom	Site	x	y	z	U_{equi}	s.o.f.
B1	16e	0.4209(3)	0.0891(3)	0.2908(3)	118(8)	1*
		0.4210(2)	0.0889(2)	0.2905(3)	96(6)	1*
		0.4202(4)	0.0884(4)	0.2989(5)	143(16)	1*
B2	16e	0.4468(2)	0.0560(3)	0.1021(3)	115(8)	1*
		0.4470(2)	0.0560(2)	0.1021(3)	92(7)	1*
		0.4470(2)	0.0560(2)	0.1021(3)	92(7)	1*
B3	16e	0.1774(3)	−0.0874(3)	0.0443(4)	116(7)	1*
		0.1775(2)	−0.0872(2)	0.0444(3)	90(6)	1*
		0.1775(2)	−0.0872(2)	0.0444(3)	90(6)	1*
B4	16e	0.3582(3)	0.1236(2)	−0.0343(3)	115(7)	1*
		0.3578(3)	0.1237(2)	−0.0333(3)	95(6)	1*
		0.3578(3)	0.1237(2)	−0.0333(3)	95(6)	1*
B5	16e	0.1998(3)	0.0575(3)	−0.0397(3)	119(8)	1*
		0.2001(2)	0.0575(2)	−0.0397(3)	97(7)	1*
		0.2002(4)	0.0578(4)	−0.0401(5)	154(16)	1*
B6	16e	0.2264(3)	0.2206(3)	0.0343(3)	120(8)	1*
		0.2268(2)	0.2208(2)	0.0341(3)	95(7)	1*
		0.2265(4)	0.2208(4)	0.0339(5)	143(16)	1*
B7	16e	0.3331(2)	0.2152(3)	0.3486(3)	117(7)	1*
		0.3330(2)	0.2154(2)	0.3484(3)	96(6)	1*
		0.3323(4)	0.2155(4)	0.3471(5)	147(16)	1*
Li1	8c	0	0	0.102(2)	199(36)	0.5(4)
		0	0	0.103(1)	188(33)	1/2
		0	0	0.063(1)	804(201)	0.17(2)
Li2	8d	0.444(2)	1/4	1/8	228(61)	0.2(1)
		0.445(2)	1/4	1/8	219(47)	0.2(1)
		0.20 (1)	1/4	1/8	627(370)	0.1(2)
Li3	16e	0.400(1)	0.103(1)	0.561(1)	250(29)	0.5(5)
		0.400(1)	0.103(1)	0.560(1)	207(24)	1/2
		0.393(1)	0.099(1)	0.562(1)	146(142)	1/2
Li4	16e	0.556(1)	0.222(1)	−0.028(1)	230(31)	0.5(7)
		0.557(1)	0.224(1)	−0.028(1)	193(25)	1/2
		0.566(4)	0.198(4)	−0.023(5)	174(142)	0.16(3)

Note. Standard deviations in parentheses.

TABLE III

U_{ij} COEFFICIENTS OF THE ANISOTROPIC TEMPERATURE FACTORS (PM^2) FOR Li_3B_{14} (FIRST ROW, CONVENTIONAL REFINEMENT; SECOND ROW, REFINEMENT FOR $2\theta \geq 30°$) AND FOR $Li_{3-x}B_{14}$ (THIRD ROW)

Atom	U_{11}	U_{22}	U_{33}	U_{12}	U_{13}	U_{23}
B1	117(13)	117(13)	121(13)	−18(11)	−3(11)	7(11)
	99(11)	88(11)	100(11)	23(9)	−1(9)	8(9)
	113(21)	124(20)	131(18)	13(17)	1(17)	−27(18)
B2	104(13)	108(13)	133(12)	−25(10)	4(12)	1(12)
	88(11)	80(12)	108(11)	25(8)	3(10)	2(10)
	168(21)	159(23)	142(20)	−37(17)	25(19)	20(19)
B3	123(13)	107(13)	116(13)	13(11)	7(11)	−10(11)
	100(11)	77(11)	93(11)	−8(9)	11(10)	−11(9)
	125(20)	128(20)	131(20)	18(16)	−8(18)	10(17)
B4	122(12)	106(13)	119(13)	−4(10)	1(11)	−8(11)
	102(11)	85(11)	99(11)	−4(8)	6(9)	−14(9)
	144(20)	110(21)	115(19)	28(15)	−3(18)	−7(17)
B5	109(13)	124(14)	124(14)	11(12)	−9(11)	−15(11)
	82(11)	105(12)	103(11)	18(10)	−9(9)	14(10)
	129(20)	133(20)	127(19)	11(17)	6(18)	−10(17)
B6	132(14)	104(13)	125(15)	−1(11)	10(11)	9(13)
	102(12)	80(11)	102(13)	2(9)	7(9)	−2(11)
	132(20)	111(19)	112(21)	6(15)	0(17)	14(18)
B7	111(13)	127(13)	113(12)	12(11)	12(12)	7(11)
	84(11)	116(11)	90(11)	24(9)	3(10)	3(10)
	136(20)	116(20)	117(19)	9(16)	2(18)	1(17)
Li1	257(68)	94(60)	245(61)	82(55)	0	0
	245(62)	115(56)	205(56)	143(48)	0	0
	804(201)	*				
Li2	494(132)	65(86)	124(93)	0	0	19(59)
	429(99)	37(61)	192(79)	0	0	33(51)
	174(142)	*				
Li3	141(44)	326(56)	283(49)	37(41)	12(46)	−39(47)
	139(38)	271(45)	212(39)	42(34)	7(39)	−17(39)
	153(65)	161(67)	147(60)	96(51)	84(60)	27(57)
Li4	137(42)	260(58)	294(58)	−25(39)	1(41)	−3(48)
	110(35)	233(49)	236(46)	61(33)	−51(36)	26(40)
	627(370)	*				

Note. Standard deviations in parentheses. * Indicates isotropic U values. The U_{ij} are defined for $\exp[-2\pi^2(U_{11}h^2a^{*2} + \cdots + 2U_{23}klb^*c^*)]$.

The composition, with respect to the X-ray data, is $Li_{2.9\pm0.1}B_{14}$. The analysis of the difference Fourier synthesis shows only very small residual density, which cannot be collected by the usual refinement procedure. These residuals might be due to 0.1 Li atoms missing at the Li2 site. But the present crystal could as well be partially deintercalated under the conditions of the chemical synthesis. The Li2 site is obviously that position which can be depopulated most easily to yield $Li_{2.5}B_{14}$. Consequently this site shows the lowest occupancy in $Li_{3-x}B_{14}$ (compare Section 5). The structural data do not allow for a discrimination between dynamic or static disorder of the lithium atoms. However, the topochemical reactions (cf. Section 5) and the ionic conductivity (cf. Section 4) indicate a considerable mobility of these atoms already at room temperature.

The structure refinement of $Li_{1.3}H_{0.4}O_{0.6}B_{14}$ from reaction (i) of Section 5 was started using the boron frame of Li_3B_{14} as initial parameters. Only slight parameter shifts occur. Of the Li atoms only the position Li3 could be identified and refined with the same occupancy as in Li_3B_{14} (Table II). The other Li positions are clearly depopulated and give rise to a composition of $Li_{1.8(4)}B_{14}$. The slightly higher Li content with respect to the chemical analysis is due to the ambiguity in the temperature factors of the Li positions and to the fact that after the reaction the presence of some H and O atoms in the structure cannot be excluded. This would of course increase the total electron density per unit cell.

7. Description of the Structure and Discussion

Li_3B_{14} represents a novel structure type. The boron atoms form two different clusters, namely the dodecahedral closo-B_8 cage and the hexadecahedral closo-B_{10} cage, which are connected via external boron–boron bonds to a three-dimensional infinite framework $^3_\infty[(B_8)(B_{10})_2]$ (Figs. 4 and 5). Each of the boron atoms is part of one of the cluster moities and is involved in one additional external bond to a neighboring cluster. The B_8 cages are centered at the special positions 4b ($00\frac{1}{2}$, etc.; $\bar{4}$ symmetry) and are connected via eight B–B bonds (B1–B7 and B2–B4; Table IV) to the eight neighboring B_{10} cages centered at the positions 8d ($x\frac{11}{48}$, etc.; $x = -0.15$; symmetry 2). The B_{10} cages form a three-dimensional 6-connected network of the type $3^34^25^1$ which

TABLE IV

INTERATOMIC DISTANCES (PM) BELOW 300 PM

B1–B7	173.5(5)	–B7	171.1(6)	B5–B3	175.0(5)	–B3	174.0(6)
–B2	174.5(5)	–B2	175.3(6)	–B3	176.6(5)	–B3	176.5(6)
–B2	178.4(5)	–B2	176.7(6)	–B4	184.4(5)	–B5	185.4(9)
–B2	182.4(5)	–B2	177.9(6)	–B4	184.8(5)	–B4	185.6(6)
–B1	195.2(5)	–B1	200.5(7)	–B5	187.1(7)	–B4	186.5(6)
–B1	195.2(5)	–B1	200.5(7)	–B6	189.7(5)	–B6	188.6(6)
–Li2	225.3(11)	–Li3	236.9(10)	–Li1	230.9(5)	–Li1	224.2(7)
–Li4	229.5(4)	–Li2	238.0(44)	–Li2	235.2(10)	–Li3	231.0(10)
–Li3	243.6(9)	–Li2	247.7(43)	–Li3	235.4(10)	–Li2	238.6(45)
–Li2	250.9(11)	–Li2	278.0(43)	–Li3	241.2(11)	–Li1	241.5(21)
–Li4	251.5(14)			–Li1	257.3(9)	–Li3	245.8(11)
–Li2	264.6(10)			–Li3	273.7(11)	–Li4	253.1(5)
						–Li3	279.1(12)
B2–B2	166.0(6)	–B4	167.7(6)			–Li4	287.5(91)
–B4	170.7(5)	–B1	175.3(6)				
–B1	174.5(5)	–B1	176.7(6)	B6–B3	171.8(5)	–B3	173.7(6)
–B1	178.4(5)	–B1	177.9(6)	–B6	174.3(6)	–B6	174.3(9)
–B1	182.4(5)	–B2	180.2(9)	–B7	178.7(5)	–B7	176.6(6)
–Li4	209.9(3)	–Li2	226.9(44)	–B4	185.8(5)	–B4	184.4(6)
–Li3	227.0(11)	–Li3	229.2(11)	–B5	189.7(5)	–B5	188.6(6)
–Li3	229.3(11)	–Li3	241.0(11)	–B7	191.1(5)	–B7	190.9(6)
–Li1	238.7(17)	–Li1	227.5(51)	–Li3	231.9(11)	–Li4	93.1(34)
–Li2	224.0(11)	–Li2	284.7(43)	–Li3	235.0(11)	–Li3	228.8(11)
–Li2	264.8(11)			–Li2	239.4(11)	–Li2	230.7(43)
				–Li2	243.5(10)	–Li3	233.0(12)
B3–B6	171.8(5)	–B4	173.4(6)	–Li4	251.8(20)	–Li2	241.1(44)
–B7	173.3(5)	–B6	173.7(6)				
–B4	174.9(5)	–B7	173.9(6)	B7 –B3	173.3(5)	–B1	171.1(6)
–B5	175.0(5)	–B5	174.0(6)	–B1	173.5(5)	–B3	173.9(6)
–B5	176.6(5)	–B5	176.5(6)	–B6	178.7(5)	–B6	176.6(6)
–Li1	218.7(5)	–Li4	208.8(55)	–B7	184.8(7)	–B4	182.0(6)
–Li3	224.3(10)	–Li1	210.5(6)	–B4	184.8(5)	–B7	183.3(9)
–Li2	227.6(11)	–Li3	226.0(10)	–B6	191.1(5)	–B6	190.9(6)
–Li1	249.6(10)	–Li2	230.1(44)	–Li2	236.7(11)	–Li2	226.6(44)
–Li3	255.1(11)	–Li1	231.5(23)	–Li3	236.9(10)	–Li3	237.9(11)
–Li3	256.3(11)	–Li3	246.3(11)	–Li4	236.9(12)	–Li2	240.5(43)
		–Li3	260.4(11)	–Li2	241.5(11)	–Li4	249.0(57)
		–Li2	296.5(44)	–Li2	258.3(11)	–Li4	252.6(12)
						–Li2	275.1(43)
B4–B2	170.7(5)	–B2	167.7(6)	Li1–Li3	173.0(13)	–Li1	112.(11)
–B3	174.9(5)	–B3	173.4(6)	–Li3	173.0(13)	–Li3	191.9(33)
–B5	184.4(5)	–B7	182.0(6)	–Li1	182.5(36)	–Li3	191.9(33)
–B5	184.8(5)	–B6	184.4(6)	–B3	218.7(5)	–B3	210.5(6)
–B7	184.8(5)	–B5	185.6(6)	–B3	218.7(5)	–B3	210.5(6)
–B6	185.8(5)	–B5	186.5(6)	–B4	227.4(9)	–B5	224.2(7)
–Li4	217.8(10)	–Li2	234.5(43)	–B4	227.4(9)	–B5	224.2(7)
–Li1	227.4(9)	–Li1	245.4(31)	–B5	230.9(5)	–B3	231.5(23)
–Li2	239.0(11)	–Li3	255.1(12)	–B5	230.9(5)	–B3	231.5(23)
–Li3	247.1(11)	–Li3	259.0(12)	–B2	238.7(17)	–B5	241.5(21)
–Li3	265.1(11)	–Li4	260.4(65)	–B2	238.7(17)	–B5	241.5(21)
–Li2	280.5(10)	–Li2	295.4(44)	–B3	249.6(10)	–B4	245.4(31)

Note. The first column refers to Li_3B_{14} and the second to $Li_{3-x}B_{14}$.

TABLE IV—*Continued*

–B3	249.6(10)	–B4	245.4(31)	–B2	229.3(11)	–B6	228.8(11)
–B5	257.3(9)	–Li2	267.3(52)	–B6	231.9(11)	–B2	229.2(11)
–B5	257.3(9)	–Li2	267.3(52)	–B6	235.0(11)	–B5	231.0(10)
–Li2	269.1(13)	–Li3	273.1(45)	–B5	235.4(10)	–B6	233.0(12)
–Li2	269.1(13)	–Li3	273.1(45)	–B7	236.9(10)	–B1	236.9(10)
		–B2	277.5(51)	–B5	241.2(11)	–B7	237.9(11)
		–B2	277.5(51)	–B1	243.6(9)	–B2	241.0(11)
				–B4	247.1(11)	–B5	245.8(11)
Li2–Li3	142.1(15)	–Li3	109.4(44)	–B3	255.1(11)	–B3	246.3(11)
–Li4	184.2(17)	–Li4	217.2(43)	–B3	256.3(11)	–B4	255.1(12)
–B1	225.3(11)	–B7	226.6(44)	–B4	265.1(11)	–B4	259.0(12)
–B3	227.6(11)	–B2	226.9(44)	–B5	273.7(11)	–B3	260.4(11)
–B5	235.2(10)	–B3	230.1(44)	–Li4	285.7(16)	–Li1	273.1(45)
–B7	236.7(11)	–B6	230.7(43)			–B5	279.1(12)
–B4	239.0(11)	–B4	234.5(43)				
–B6	239.4(11)	–B1	238.0(44)	Li4–Li2	184.2(17)	–B6	93.1(34)
–B7	241.5(11)	–B5	238.6(45)	–Li2	184.2(17)	–B6	93.1(34)
–B6	243.5(10)	–B7	240.5(43)	–B2	209.9(3)	–Li3	196.0(48)
–B2	244.0(11)	–B6	241.1(44)	–B2	209.9(3)	–Li3	196.0(48)
–B1	250.9(11)	–B1	247.7(43)	–B4	217.8(10)	–B3	208.8(55)
–B7	258.3(11)	–Li1	267.3(52)	–B4	217.8(10)	–B3	208.8(55)
–B1	264.6(10)	–B7	275.1(43)	–B1	229.5(4)	–Li2	217.2(43)
–B2	264.8(11)	–B1	278.0(43)	–B1	229.5(4)	–Li2	217.2(43)
–Li1	269.1(13)	–B2	284.7(43)	–B7	236.9(12)	–B7	249.0(57)
–Li2	280.3(18)	–Li2	286.7(89)	–B7	236.9(12)	–B7	249.0(57)
–B4	280.5(10)	–B4	295.4(44)	–B1	251.5(14)	–B7	252.6(12)
		–B3	296.5(44)	–B1	251.5(14)	–B7	252.6(12)
				–B6	251.8(20)	–B5	253.1(5)
Li3–Li2	142.1(15)	–Li2	109.4(44)	–B6	251.8(20)	–B5	253.1(5)
–Li1	173.0(13)	–Li1	191.9(33)	–Li3	285.7(16)	–B4	260.4(65)
–B3	224.3(10)	–Li4	196.0(48)	–Li3	285.7(16)	–B4	260.4(65)
–B2	227.0(11)	–B3	226.0(10)			–B5	287.5(91)

yields from an idealized (3, 10) net by the parameter shift $x = -0.25 \rightarrow x = -0.15$ at position 8d. This corrugation allows exactly the symmetry adapted selection of 6 neighboring B_{10} cages out of 10, which is necessary to connect each B_{10} unit with 6 other B_{10} units via 6 external B–B bonds (B3–B5, B6–B6′) in addition to the 4 external B–B bonds to 4 B_8 cages (Fig. 5). The mean distances between the cage centers are 470 pm (B_8–B_{10}) and 500 pm (B_{10}–B_{10}), respectively. A very important detail of the boron framework is the helical arrangement of the B_8 units which follows in principle 4_1 screws and which is wound around the B_{10}–B_{10} connected chains along [001]. This way, spiral-like channels are created ($c/2$ shift from position 4b to 4a) in which the most preferable positions are occupied by the Li atoms in a rather uniform distribution of 50% occupancy per site. The channel dimensions allow a helical movement of the Li atoms in the [001] direction, which is also indicated by the anisotropic temperature factors of Li and by residual electron densities between the Li positions (cf. Section 6).

The B_8 and the B_{10} clusters were not observed until now in Zintl compounds, but they are well known from the boranes and correspond to the 8- and 10-fold connectivity of the units B_8H_8 and $B_{10}H_{10}$, respec-

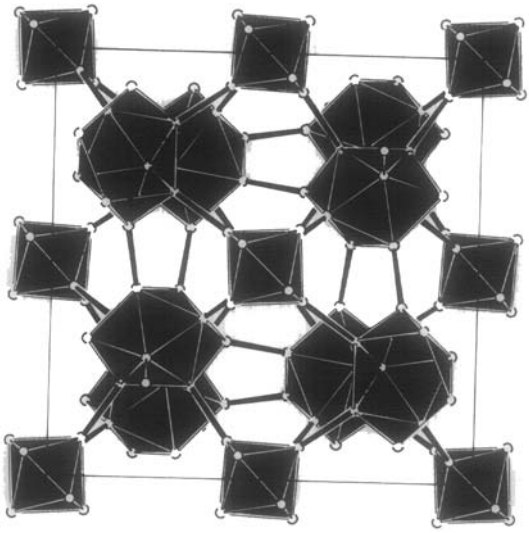

FIG. 4. View of the structure of Li_3B_{14} in [001] projection (Li atoms omitted). The B_8 (around $00\frac{1}{2}$, etc.) and B_{10} polyhedra (around $-0.15\frac{1}{18}$) are emphasized by black faces (the two uppermost B_{10} polyhedra are cut at the top). The intracluster bonds are drawn open and the intercluster bonds are filled in black.

tively. According to Wade's rules (*34*), these closo clusters require two additional electrons to fill the bonding cluster states, yielding $B_8H_8^{2-}$ and $B_{10}H_{10}^{2-}$. To accomplish this in the 3D frame of $Li_3B_{14} \hat{=} Li_6B_{28} = Li_6(B_8)(B_{10})_2$, one needs exactly the six electrons of the six Li atoms to fulfill the electronic rules: $(Li^+)_6[B_8^{2-})(B_{10}^{2-})_2]$. The electron transfer corresponds to the simple counting scheme of Zintl (*5*), Klemm (*6*), and Mooser and Pearson (*7*), but only if the electron numbers for the boron cages, given by Wade (*34*), are taken into account. The properties predicted by these rules fit completely the experimental data of the red-transparent diamagnetic semiconductor Li_3B_{14}.

The intracluster bonds range from 166.0 to 195.2 pm in the B_8 dodecahedron and from 171.8 to 191.1 pm in the B_{10} hexadecahedron. The mean value $\bar{d}_8$(B–B) = 179.8 pm of the B_8 group is slightly smaller than the value $\bar{d}_{10}$(B–B) = 181.5 pm of the B_{10} group. Both mean distances are considerably larger than the intercluster bond distances (170.7–175.5 pm; $\bar{d}$ = 173.5 pm). In fact, only the latter ones are two electron, two center bonds while the former ones arise from multicenter cluster states. It can be shown that this is true for many borides and gallides (*3*, *14*, *15*). Consequently, the highest peaks in the difference Fourier synthesis of approximately 0.11 e/Å^{-3} are located on these intercluster connections. Similar observations are reported for some other boron compounds (*35*).

Table IV shows that the distances between boron atoms and all of the Li sites are in a reasonable range. With respect to the refined site occupation factors at the Li positions one calculates an effective coordination B–Li of about CN2 to CN3. Further discussions on this subject do not seem justified.

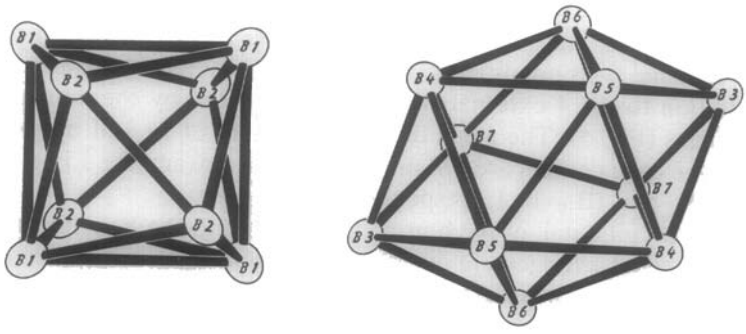

FIG. 5. B_8 (left) and B_{10} cluster (right) in Li_3B_{14} (all terminal bonds omitted).

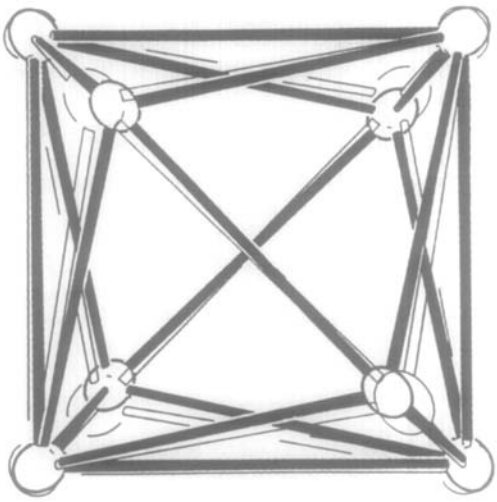

FIG. 6. Geometrical differences in the B_8 cluster in Li_3B_{14} (black polyhedron) and $Li_{1.8}B_{14}$ (open lines). The most pronounced change occurs at the B2–B2 bond (front diagonal) which is expanded from 166 pm (Li_3B_{14}) to 176 pm ($Li_{1.8}B_{14}$).

During the course of the reaction from Li_3B_{14} to $Li_{1.3}(H_{0.4}O_{0.6})B_{14}$ a decrease of the unit cell volume of about 15 Å^3 is observed. This relatively small change is due to competing factors, namely the lithium loss versus geometry preservation of the boron frame. The mean B–B bond lengths 182.3 pm (intra B_8), 180.1 pm (intra B_{10}), and 171.7 pm (intercluster) show very small but significant changes as compared with the Li_3B_{14} values. This is also true for the local changes (Fig. 6). Only one triangle of the B_8 cage (B2–B2–B1) changes considerably. The very short distance B2–B2 = 166.0 pm increases to 177.9 pm, while B1–B2 = 174.5 and 178.4 pm change to 175.3 and 176.7 pm, respectively. It is very likely that the change of d(B2–B2) is due to an oxidation of the B_8 cage. Figure 7 displays the B_8 cluster including terminal bonds together with deformation density distributions for Li_3B_{14} (Fig. 7, left) and $Li_{1.8}B_{14}$ (Fig. 7, right) (0.015 e/Å^3 each). Despite the fact that the deformation density of $Li_{1.8}B_{14}$ is principally distorted with respect to Li_3B_{14} there is a significant decrease in the electron density in the neighborhood of the B2–B2 bonds. This observation can only be

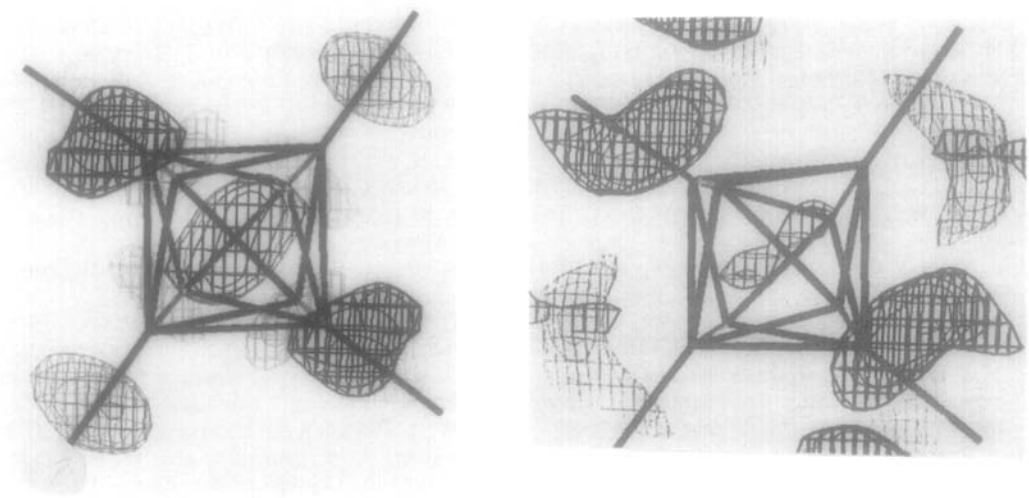

FIG. 7. Deformation electron density according to the present X-ray data, which shows the surfaces of 0.015 e/Å in the region of the B_8 cluster in Li_3B_{14} (left) and $Li_{1.8}B_{14}$ (right). The pronounced electron densities at the terminal bonds are distorted under the topotactical reaction ($a \rightarrow b$), but do not vanish like the electron densities at the surface of the B_8 polyhedron. This is in agreement with the assumption that the B_8 cluster undergoes the redox reaction.

taken as a weak support of our assumption that only the B_8 cage is oxidized under the topotactical reaction. More detailed investigations have to be done. A remarkable change is observed in the Li channels. After the reaction the nonboron electron density distribution is much more ambiguous. Only one of the former Li positions can still be identified as such (Table III). It is sure by comparison with experiments (ii) and (iii) that lithium can be extracted from Li_3B_{14} without introducing other elements into the structure. But it is not clear from the X-ray data whether the positions Li1, Li2, and Li4 are exclusively depopulated or whether foreign atoms (O, H) are incorporated into the structure, as well as under the conditions of reaction I.

References

1. H. G. VON SCHNERING, *Angew. Chem. Int. Ed. Engl.* **93,** 44 (1987); J. D. CORBETT, *Chem. Rev.* **85,** 383 (1985).
2. H. SCHÄFER, B. EISENMANN, AND W. MÜLLER, *Angew. Chem.* **85,** 742 (1973); *Angew. Chem. Int. Ed. Engl.* **12,** 694 (1973); H. SCHÄFER AND B. EISENMANN, *Rev. Inorg. Chem.* **3,** 29 (1981).
3. H. SCHÄFER, *Annu. Rev. Mater. Sci.* **15,** 1 (1985).
4. H. G. VON SCHNERING, *Nova Acta Leopold. 264* **59,** 165 (1985), *Bol. Soc. Chil. Quim.* **33,** 41 (1988).
5. E. ZINTL, *Angew. Chem.* **52,** 1 (1939).
6. W. KLEMM, *Proc. Chem. Soc. London,* 329 (1958); W. Klemm, "Festkörperprobleme," Vol. III, Vieweg, Braunschweig (1963).
7. E. MOOSER AND W. B. PEARSON, *Phys. Rev.* **101,** 1608 (1956).
8. M. C. BÖHM, R. RAMIREZ, R. NESPER, AND H. G. VON SCHNERING, *Phys. Rev. B* **30,** 4870 (1984).
9. M. C. BÖHM, R. RAMIREZ, R. NESPER, AND H. G. VON SCHNERING, *Ber. Bunsenges. Phys. Chem.* **89,** 465 (1985).
10. R. RAMIREZ, R. NESPER, H. G. VON SCHNERING, AND M. C. BÖHM, *Chem. Phys.* **95,** 17 (1985).
11. R. RAMIREZ, R. NESPER, H. G. VON SCHNERING, AND M. C. BÖHM, *Z. Naturforsch. A* **41,** 1267 (1986).
12. R. RAMIREZ, R. NESPER, H. G. VON SCHNERING, AND M. C. BÖHM, *J. Phys. Chem. Solids* **48,** 51 (1987).
13. R. THÜMMEL AND W. KLEMM, *Z. Anorg. Allg. Chem.* **376,** 44 (1970).
14. J. STÖHR AND H. SCHÄFER, *Rev. Chim. Miner.* **19,** 122(1982).
15. C. BELIN AND R. G. LING, *J. Solid State Chem.* **48,** 40 (1983).
16. D. R. SECRIST, *J. Amer. Ceram. Soc.* **50,** 520 (1967).
17. S. DALLEK, D. W. ERNST, AND B. F. LARRIK, *J. Electrochem. Soc.* **126,** 866 (1979).
18. V. P. SOROKIN, P. J. GAVRILOV, AND E. V. LEVAKOV, *Russ. J. Inorg. Chem. (Engl. Transl.)* **22,** 329 (1977).
19. S. D. JAMES AND L. E. DEVRIES, *J. Electrochem. Soc.* **123,** 321 (1976).
20. F. E. WANG, *Trans. Amer. Inst. Metall. Pet. Eng.* **10A,** 343 (1979); cf. *J. Less-Comm. Metals* **61,** 237 (1978).
21. V. J. MATKOVICH, Ed., "Boron and Refractory Borides," Springer, Berlin (1977).
22. G. MAIR, Thesis, University of Stuttgart (1984); G. MAIR, R. NESPER, AND H. G. VON SCHNERING, "Proceedings, International Conference on Reactivity of Solids, Dijon" (1984); Annual Report Max-Planck-Institute, FKF, Stuttgart (1984).
23. K. YVON, W. JEITSCHKO, AND E. PARTHÉ, *J. Appl. Crystallogr.* **10,** 73 (1977).
24. J. D. RAISTRICK AND R. A. HUGGINS, "Proceedings, Symposium Workshop on Advanced Battery Research and Design," Argonne Natl. Lab., B-277 (1976).
25. B. SCHOCH, A. RABENAU, W. WEPPNER, AND H. HAHN, *Z. Anorg. Allg. Chem.*; W. WEPPNER, private communication.
26. K. KINKOLLA AND C. WAGNER, *J. Electrochem. Soc.* **104,** 308 (1957).
27. C. J. WEN, B. A. BONCAMP, R. A. HUGGINS, AND W. WEPPNER, *J. Electrochem. Soc.* **126,** 2258 (1979).
28. R. N. SEEFURTH AND R. A. SHARMA, *J. Electrochem. Soc.* **122,** 1049 (1975).
29. J. R. HEUS AND J. J. EGON, *J. Phys. Chem.* **77,** 1989 (1973).
30. K. YVON, W. JEITSCHKO, AND E. PARTHÉ, *J. Appl. Crystallogr.* **10,** 73 (1977).
31. G. SHELDRICK, "SHELXS Crystal Structure Solution Program," Göttingen (1985): G. Sheldrick, "SHELX 76, Crystal Structure Solution and Refinement Program," Göttingen (1976).
32. W. R. BUSING, K. O. MARTIN, H. A. LEVY, G. M. BROWN, C. K. JOHNSON, AND W. E. THISSEN, "ORFFE3, Crystallographic Function and Error Program," Oak Ridge (1971).
33. C. K. JOHNSON, "ORTEPII, Thermal Ellipsoid Plot Program," Oak Ridge (1976).
34. K. WADE, *Adv. Inorg. Chem. Radiochem.* **18,** 1 (1976).
35. A. KIRFEL, A. GUPTA, AND G. WILL, *Acta Crystallogr. Sect. B* **35,** 1052, 2291 (1979); **36,** 1311 (1980).